Engineering Structures 82 (2015) 22–32

Contents lists available at ScienceDirect

Engineering Structures

journal homepage: www.elsevier.com/locate/engstruct

Experimental and numerical analysis to collapse of a framed structure subjected to seismic loading

Martín Domizio, Daniel Ambrosini *, Oscar Curadelli

Structural Engineering Master Program, Engineering Faculty, National University of Cuyo, Mendoza, Argentina
CONICET, National Research Council, Argentina

ARTICLE INFO

Article history:
Received 25 April 2014
Revised 9 October 2014
Accepted 10 October 2014
Available online 1 November 2014

Keywords:
Nonlinear dynamic analysis
Collapse
P-Delta effect
Experimental test
Shaking table
Calibration

ABSTRACT

The nonlinear numerical analysis to collapse of civil structures presents several difficulties, even for mechanically well-characterized materials, such as steel. In the case of steel, where the nonlinear constitutive equation is one of the simplest and best known, in many cases there are large differences when the numerical analysis and experimental results are compared. In this paper, the results of an experimental and numerical analysis of a single degree of freedom (SDOF) steel structure are presented. The structure was subjected to near fault earthquakes that caused nonlinear behavior of their components and structural collapse. The experimental model was tested on a shaking table. Complementary tests were performed to characterize the properties of the steel employed, and thus define the parameters used in the numerical simulation. After the calibration of the nonlinear material model, a comparison is made between the experimental and numerical results obtained. Finally, a numerical study, following the modeling methodology obtained from the numerical–experimental analysis, is performed to quantify the influence of the P-Delta effect on the structural collapse.

1. Introduction

One of the main objectives of the structural engineering is to prevent the collapse of structures in order to preserve the life of the occupants. Consequently, it is important, both in the design of new structures and in the assessment and rehabilitation of existing structures, to know the safety margin against collapse.

The collapse can be defined as the loss of the ability to support vertical loads by the structure. In practice, there have been direct vertical collapses and collapses with large lateral displacements. The first of them arises when one or more structural elements lose their bearing capacity suddenly, while the second type is observed when dynamic instability is reached, with large horizontal displacements and large story drifts. This latter type of collapse can be classified as instability-type collapse, according to the typology proposed by Starossek [1].

The action of gravity loads over a laterally deformed structure causes an increase in the member forces and in the lateral deflections while it reduces the resistance to lateral loads. This process is known as P-Delta effect, and may lead to negative values of stiffness in the inelastic response of flexible structures. If the displacement demand of the seismic action is high enough the structure can reach dynamic instability and collapse [2].

At present, there are different methods to evaluate the safety of structures against the collapse produced by the seismic action. Villaverde [3] have performed a comprehensive review of these methods, and concludes that the nonlinear dynamic analysis of the entire structure, modeled using finite elements, is the most reliable method for evaluating the collapse. However this method has the disadvantage of being computationally expensive. The author also states that the following considerations should be taken into account: the model must solve the equation of motion in the deformed configuration, elements that are compatible with large deformations should be employed, the mesh should be fine enough to faithfully reproduce the structural behavior in zones that undergo inelastic strains, and finally simulations must be performed with several seismic records to obtain meaningful information about the structural collapse. In any case, the material models and numerical codes should be carefully calibrated against experimental tests.

Alternatively, concentrated plasticity models that represent phenomenologically the nonlinear behavior of structural elements have been used in recent studies [4–7]. These models take into account fundamental aspects such as the degradation of strength and stiffness, both on steel and on reinforced concrete elements, and have been calibrated through many tests of cyclic loading

* Corresponding author at: Facultad de Ingeniería, Centro Universitario, Parque Gral. San Martín, 5500 Mendoza, Argentina. Fax: +54 261 4380120.
E-mail address: dambrosini@uncu.edu.ar (D. Ambrosini).

http://dx.doi.org/10.1016/j.engstruct.2014.10.022
0141-0296/

[8,9]. At the same time, complete structure models were validated with experimental test results [10,11]. The use of such models allows a large number of simulations to be performed, in which the effects on the structural collapse due to the variability of the seismic action and the properties of the structure can be studied.

The structural instability under seismic loading has been studied, both at numerical and analytical levels, by several authors [12–14]. Miranda and Akkar [15] have studied the dynamic instability in SDOF systems, with bilinear hysteretic behavior and negative post-yielding slope. In this study, nonlinear dynamic analyses to collapse were performed on structures with different fundamental periods and several negative post-yielding slopes. The results of this analysis shown that dynamic instability is reached more readily in structures with more pronounced negative post-yielding slope and lower fundamental periods.

Shafei et al. [16] conducted a statistical study on the collapse of moment resistant frame and shear wall structural systems, with diverse structural parameters, subjected to seismic excitations. From the results of this study mathematical models were obtained using multivariate regression analysis. Based on the mathematical models, collapse fragility curves can be established in order to estimate the probability of the structural collapse. This probability is calculated as a function of the dynamic properties and the non-linear properties of the structure, estimated from a pushover analysis.

Adam and Jäger [17] have proposed to evaluate the vulnerability of structures with the sign of the post-yield tangent stiffness obtained from a nonlinear static analysis. From results of incremental dynamic analysis it was observed that the structural collapse is reached more readily when the structure has a pronounced negative post-yield tangent. The authors also have defined a collapse capacity spectrum to estimate earthquake intensity that produces the collapse of a structure with a given fundamental period and a post-yield stiffness. The structure analyzed with this method must be regular to be well represented by the equivalent SDOF system, and should not have resistance or stiffness degradation.

The collapse of structures induced by earthquakes has been studied experimentally in a lesser extent [18–22]. Vian and Bruneau [23] have performed experimental tests over several SDOF structures under seismic forces, which were increased to collapse level. The structures tested had different slenderness and mass, and they show no degradation. From the results of this test, it was observed that the traditional stability factor (a measure of the importance of P-Delta effect) indicates what structures are more vulnerable to collapse. The results of these tests also showed that the higher the influence of P-Delta effect, the lower plastic strains and displacements that are achieved when dynamic instability occurs.

Lignos and Krawinkler [24] have conducted an experimental and analytical study of two four-story steel frames under seismic forces that cause collapse. Plastic strains of the structure were concentrated in hinges specially designed, which were characterized in cyclic tests. On the basis of the results obtained it is concluded that the P-Delta effect and degradation in plastic hinges are the factors that define the behavior of the structures when they are near collapse.

Lignos et al. [25] have made an analysis of the numerical models employed to reproduce the full scale test of a 4-story steel frame. The test was performed on the E-Defense shaking table in Japan in 2007 [26] as part of a contest that was aimed to assess the responses of various analytical models. These responses were ordered according to their similarity to the structural response measured experimentally. From the results of the contest, it was concluded again that in order to obtain reliable results, P-Delta effect and degradation of strength and stiffness of structural elements must be taken into account explicitly in the numerical model.

The main objectives of this paper are to evaluate the effectiveness of a numerical model to replicate the experimental collapse of a SDOF structure that does not have strength or stiffness degradation, and to provide insight on the influence of P-Delta effect in the collapse of framed steel structures subjected to near fault earthquakes. For this purpose, experimental tests were conducted on steel-frame structures using a shaking table. The paper includes a brief description of the dynamic actions employed, additional tests performed, and the experimental and numerical models of the tested structures. After this, the calibration of the numerical model is shown and the comparative results of both models are presented along with the conclusions. Finally, a numerical study, following the modeling methodology obtained from the numerical–experimental analysis, is performed to quantify the influence of the P-Delta effect on the structural collapse. It is worth mentioning that the conclusions obtained in this work are limited to flexible structures without strength or stiffness deterioration, as the structure studied in this case reaches the collapse by dynamic instability prior to suffer effects such as local buckling, lateral torsional buckling or material degradation due to fatigue phenomena.

2. Experimental model

The model employed in this work is a frame structure, in which the columns were made of steel flat bars and the beam was made of rectangular steel tube filled with lead to achieve mass values desired. The high bending stiffness of the beam produced a restriction on the rotation of the column ends, thereby forming a SDOF system. Fig. 1 shows the geometry of the model.

In the experimental tests, two models with different column heights and mass in the beam were employed, adopting the values shown in Table 1. These values were chosen in order to obtain

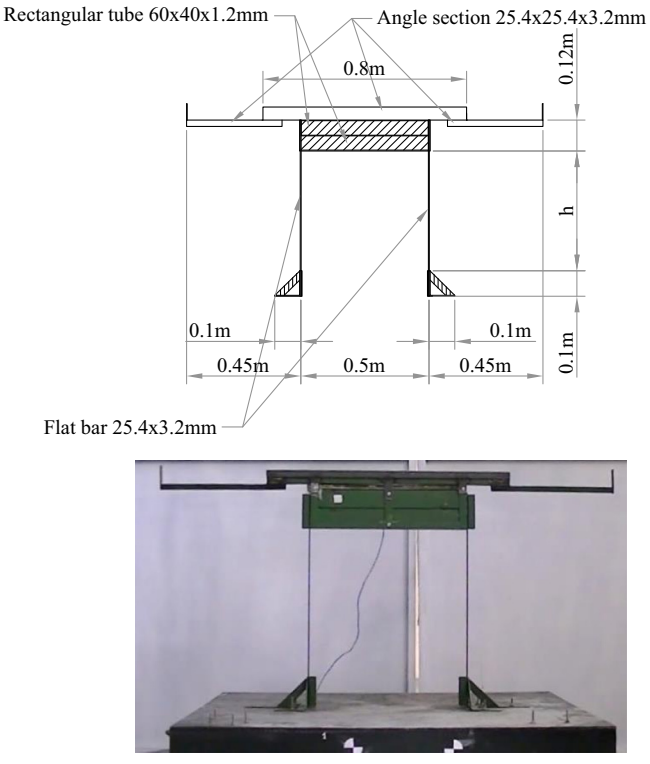

Fig. 1. Experimental model.

Table 1
Properties of the experimental models.

Model	Column height (m)	Beam mass (kg)	Fundamental frequency (Hz)	Lateral stiffness (N/m)		Stability factor
				w/o P-Delta effect	w/P-Delta effect	
A	0.52	25.4	1.29	2147.9	1668.7	0.22
B	0.47	33.4	1.28	2853.1	2160.4	0.24

similar frequencies in the fundamental modes of the two structures. This allowed observing the response of structures with high influence of P-Delta effect. The influence of this effect increases as the stability factor of the structure increases. Normally [27], this factor is defined according to Eq. (1), and the influence on the lateral stiffness is quantified according to Eq. (2).

$$\theta = \frac{P}{K_0 \cdot L} \tag{1}$$

$$K_1 = K_0 \cdot (1 - \theta) \tag{2}$$

where θ is the stability factor, P is the axial load on the columns, K_0 the elastic bending stiffness ignoring the P-Delta effect, K_1 the elastic bending stiffness taking into account the P-Delta effect, and L the column height.

The properties of the two models employed in this study are shown in Table 1. The fundamental frequency was measured in free vibration test that were performed before and after each forced vibration test. From this measured frequency and the value of the beam mass and column height, the lateral stiffness and stability factor were calculated. Also, from the free vibration tests, damping ratios of 0.42% and 0.44% were estimated for the model A and model B respectively. Free vibration tests made after shaking table tests showed no changes in the fundamental frequency, despite large plastic deformations were observed in the structure. This indicates that the structure did not undergo degradation in stiffness.

In order to measure the dynamic response, capacitive accelerometers PCB Piezotronics 3701D1FA3G were employed, with a sensitivity of 700 mV/g and a measuring range of ±3 g. These devices were placed on the shaking table and at one end of the beam of the model. The accelerometers were connected to signal conditioners PCB Piezotronics 478A01. The signal was digitized by a data acquisition board PC-CARD-DAS16/16 and HP VEE 6.0 software was employed to record the time history response.

Again, it should be emphasized that the experimental models only can capture global dynamic instability as mechanism of failure. Strength and/or stiffness degradation are not considered due to local and lateral torsional buckling instability modes cannot occur in the models.

3. Seismic loading

In order to perform the experimental–numerical study, two different acceleration records were employed. Details of these records are shown in Table 2.

Accelerations, velocities and displacements of the two records are shown in Fig. 2. These records were measured in the vicinity of the fault rupture. At the beginning of the records, very noticeable displacement pulses can be observed, that is a feature of the near-fault records with forward directivity effect. It is also observed that these pulses occur almost simultaneously with the maximum values of acceleration and velocity.

Table 2
Details of the near-fault seismic records employed.

Event	Year	Station	Component	Moment magnitude	Mechanism	Distance to rupture plane (km)
Cape Mendocino	1992	Petrolia	90	7.0	Reverse	8.2
Kobe	1995	KJMA	90	6.9	Strike-slip	1.0

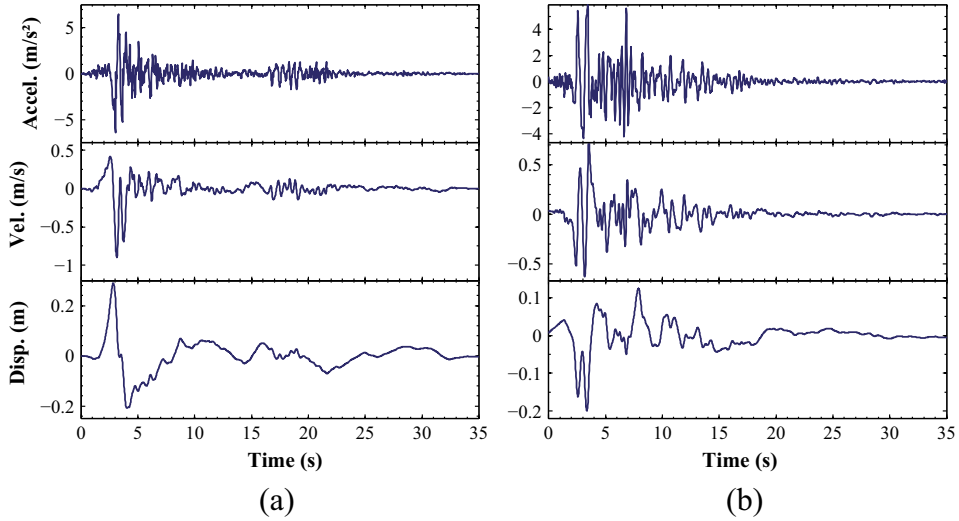

Fig. 2. Acceleration, velocity and displacement records of the ground motions employed (a) Cape Mendocino1992, Petrolia and (b) Kobe 1995, KJMA.

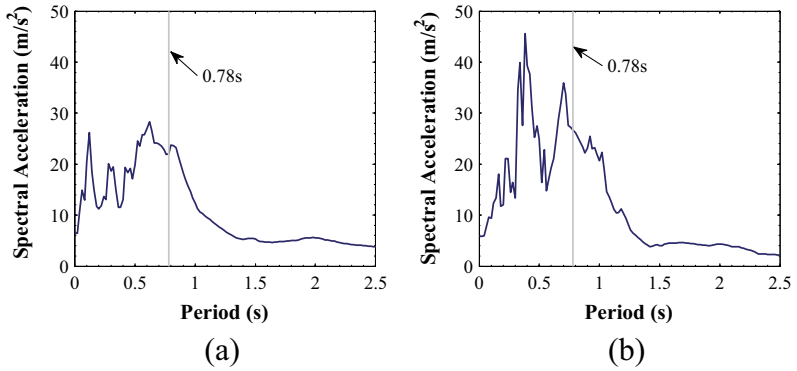

Fig. 3. Spectral acceleration of the ground motions employed (a) Cape Mendocino1992, Petrolia and (b) Kobe 1995, KJMA.

Table 3
Tests performed.

Test	Model	Record
1	A	Cape Mendocino 1992, Petrolia
2	B	Kobe 1995, Kajima

The acceleration response spectra of the two earthquakes are presented in Fig. 3, which also shows the fundamental period of the structure. It can be observed in Fig. 3 that the structure is near resonance in case of Cape Mendocino earthquake, and is in a zone of high values of spectral acceleration in the case of Kobe earthquake.

The seismic records were applied to the experimental models by mean of a shaking table with 6 degrees of freedom (MOOG 6DOF2000E). The limits of displacement, velocity and acceleration of the shaking table are 0.259 m, 0.5 m/s and 5.89 m/s^2 respectively. Because of this, the seismic record of Cape Mendocino was applied with a scaling factor of 0.83 to adapt their peak values to the limits of the shaking table.

With the change in the amplitude of Cape Mendocino record, the spectral acceleration corresponding to the fundamental period of the structure is 18.28 m/s^2, while for the Kobe record is 26.5 m/s^2. Moreover, as it can be seen in Table 3, Cape Mendocino earthquake was employed on the model A, on which P-Delta effect has less influence, allowing the structure to remain in the elastic range during experimental testing. On the other hand, when the Kobe seismic record was employed, the structure experienced large plastic deformations and finally it collapsed.

4. Numerical model

The numerical models employed in this study were performed with the software ANSYS 13 [28]. The model geometry was defined following the scheme of Fig. 1, using shell finite elements. The element type selected was SHELL181, a four node element with six degrees of freedom at each node. This type of element is suitable for use in analyzes where nonlinear materials are employed and there are large deformations and rotations. The stiffness of the selected shell element is updated at each time step from the numerical integration of the stresses, calculated independently in 5 points located through the element thickness.

In order to obtain the time history response the Newmark method, an implicit time integration scheme, was used with an automatic time step. The starting and the maximum time step were defined as 0.005 s, equal to the time step of the experimental acceleration records. The Newton–Rhapson method was employed

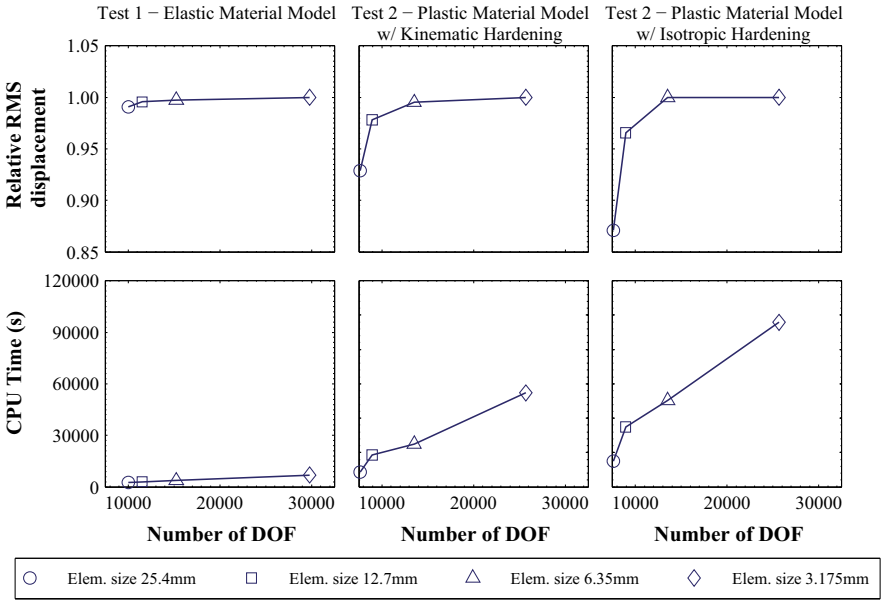

Fig. 4. Mesh sensitivity study.

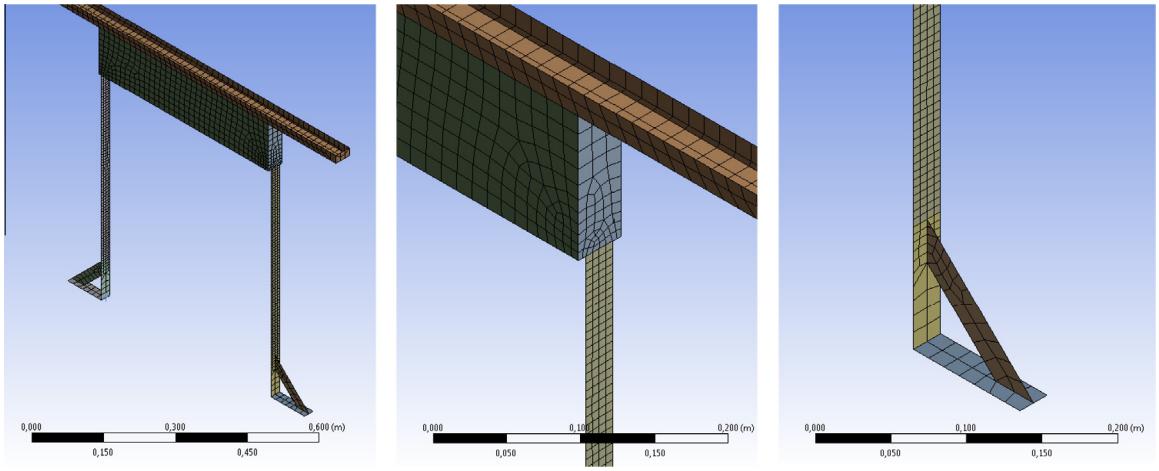

Fig. 5. Finite element mesh of the numerical model.

to solve the nonlinear equations, with a convergence tolerance of 0.5% of the Euclidean norm of the residual force vector.

The material model was defined as nonlinear steel with a bi-linear stress–strain relationship. Kinematic and isotropic hardenings were employed in order to know which is able to reproduce better the experimental response. Even if there exist material models that combine these two types of hardening [29,30], in this work they were studied separately to simplify the calibration process. Parameters defined in this material were: modulus of elasticity, yield stress and strain hardening modulus. The values adopted for these parameters were obtained from additional tests and calibration of the numerical model, as described below. Besides the material nonlinearity, geometric nonlinearity was taken into account in the numerical model due to the large displacements experienced by the structure. The seismic loading was defined as an acceleration field acting on the inertial masses of the structures, considered with a fixed support in the base. Meanwhile, the inherent structural damping was defined as proportional to the stiffness, with those values obtained from the free vibration tests described in Section 2.

In order to analyze the influence of the mesh density in the results, models with 4 different element sizes in the columns (25.4, 12.7, 6.35 and 3.175 mm) were used for the calibration and the numerical–experimental comparison described in later sections. Fig. 4 shows the root mean square (RMS) value of the displacements of the different calibrated models. These results are expressed relative to the displacements obtained from the numerical models with the highest mesh density. This figure also shows the CPU time spent in each analysis, taking into account that they were performed on a PC with an Intel Core i7-4770 processor, and that the time shown in the figure is the CPU time summed across all threads.

As it can be seen in Fig. 4, the results of the nonlinear models showed higher sensitivity to the mesh density, with CPU time consumption considerably greater compared to the linear numerical model. The results of the model with an element size of 6.35 mm have less than 1% of difference with those obtained from the model with the highest mesh density. Due to this, and to present the results in summarized form, in the rest of the paper only the results obtained from the models with an element size of 6.35 mm are shown. The numerical model meshed with this element size can be observed in Fig. 5.

It is interesting to note that for the same number of DOF, the CPU time consumption is considerably higher when isotropic hardening is used compared with kinematic hardening.

5. Material tests

Large plastic deformations and structural collapse were observed in test 2. In order to know the yield stress and tensile strength of the material employed, tensile tests were performed on the damaged columns. The specimens were built from the central portion of the column, which suffered no permanent deformation, according to the ASTM A-370 and were tested to failure on a universal testing machine AMSLER. A summary of the results is presented in Table 4.

The modulus of elasticity was calculated from a series of free vibration tests of a bar which had a known length and mass, and that was fixed at one end and free at the other. With a laser displacement sensor Microepsilon 1607, arranged according to the diagram in Fig. 6, the displacements at the free end were measured and the frequency of the first mode was obtained. Then the modulus of elasticity was calculated using Eq. (3), derived from the expression of the first mode frequency of the bar [31].

Table 4
Tensile test results.

Test	Model	Yield stress (MPa)		Tensile strength (MPa)	
		Left column	Right column	Left column	Right column
2	B	376	440	492	538

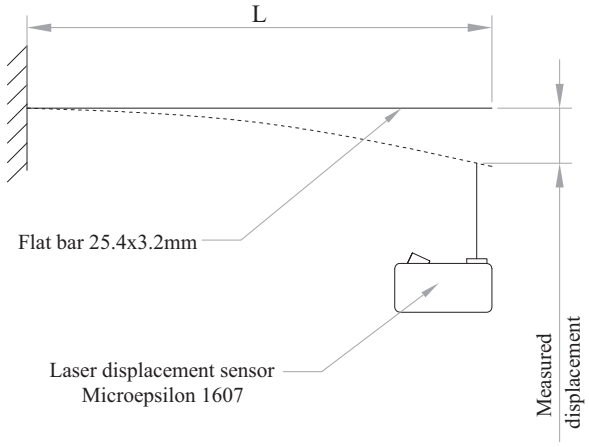

Fig. 6. Scheme of displacement measurement.

$$E = \omega^2 \cdot \frac{\bar{m} \cdot L^4}{I} \cdot \frac{1}{1.875^4} \quad (3)$$

In this expression E is the elastic modulus, $\bar{m}$ is distributed mass of the bar, L is its length, I the moment of inertia of the bar section and ω is the natural frequency measured. The results for various lengths are shown in Table 5, whereas displacements measured and Fourier amplitude of two cases are shown in Fig. 7. The mean value of the test results, 208 GPa, was adopted for the numerical model.

Table 5
Elastic modulus estimation.

Bar length (m)	Measured frequency (Hz)	Elastic modulus (GPa)
0.931	3.07	211
0.991	2.69	208
1.048	2.41	208
1.101	2.17	206
1.186	1.88	208
	Mean value	208

6. Material model calibration

In order to know the value of the strain hardening modulus that produces the best numerical approximation, a parametric study was performed by changing the value of this material property in the numerical model of the structure employed in test 2.

The actions employed in the numerical models were the acceleration recorded in the shaking table during test 2, and the values of yield stress and modulus of elasticity of material model were those described in the previous section.

In Fig. 8 the relative acceleration of the beam obtained from the numerical model is presented for both types of hardening models studied, with two values of strain hardening modulus in each case. Henceforth, the value of the strain hardening modulus is represented by a percentage α of the modulus of elasticity of the material.

The figure shows the high influence of the strain hardening modulus on the response of the numerical model. When the studied parameter is defined with relatively low values, the collapse occurs at a time previous to that recorded experimentally, which

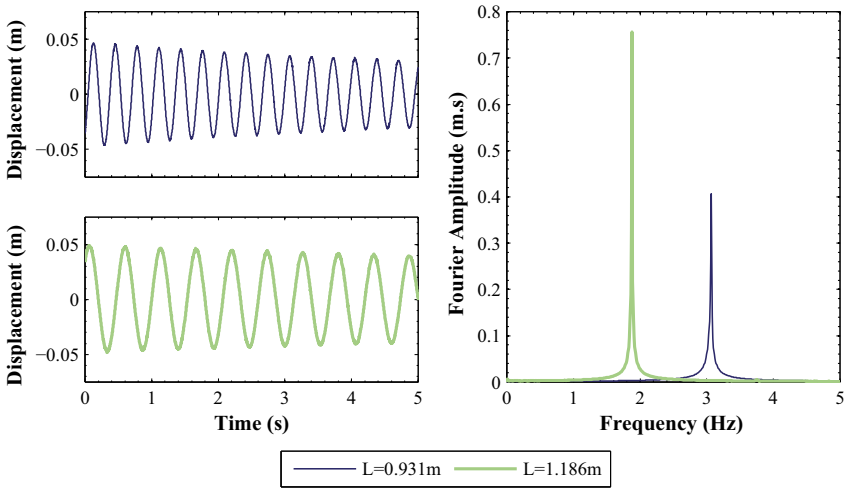

Fig. 7. Results of free vibration test.

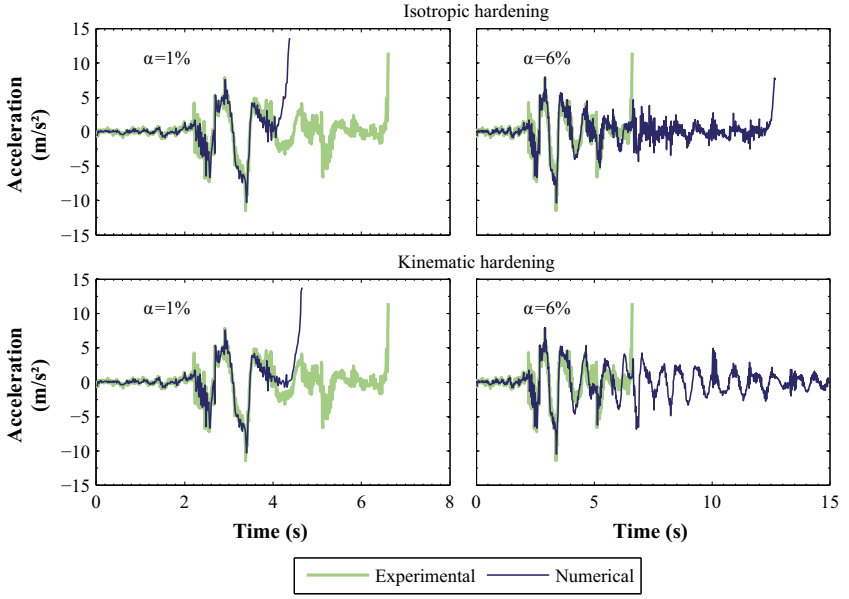

Fig. 8. Experimental–numerical comparison for various values strain hardening modulus.

is 6.54 s. On the other hand, for high values of the parameter, structural collapse does not occur.

Different results are also observed when the response with both types of hardening is compared. With equal strain hardening modulus value, the model in which hardening was defined as isotropic reaches the structural collapse faster than the model in which kinematic hardening is used. A comparison of the final deformation of the experimental and numerical model, once the collapse is reached, is shown in Fig. 9.

In order to establish the degree of similarity that exists between the experimental and numerical responses, two criteria were employed. The first is the evaluation of the normalized cross-correlation between the acceleration records obtained in each experimental test and the different responses obtained from the numerical models by varying the studied parameter. This coefficient varies between −1 and 1, taking the value 1 if the two signals are exactly equal and they have the same sign, −1 when two signals are equal with opposite sign and an intermediate value closer to 0 for the larger the differences between the signals. The value of the normalized cross-correlation is calculated according to Eq. (4).

$$R = \frac{\sum_i a_{\exp}[t_i] \cdot a_{num}[t_i]}{\sqrt{\sum_i a_{\exp}[t_i]^2 \cdot \sum_i a_{num}[t_i]^2}} \tag{4}$$

where $a_{exp}[t_i]$ is the value of the experimentally measured acceleration at time t_i and $a_{num}[t_i]$ is the acceleration value obtained from the numerical model at the same time. The cross correlation coefficient is a measure of the shape similarity between two time records, but it is not a sensitive indicator of the amplitude difference between the records. For this reason, comparison of the RMS values of the two records was employed as the second criterion.

Fig. 10 shows the variation of the two indicators as a function of the strain hardening modulus defined in the numerical simulations. The figure also shows with dashed line the values adopted for the parameter, which are those that give the largest value of cross-correlation coefficient in each of the cases.

Fig. 10 shows that there is a value of strain hardening modulus for which the cross-correlation coefficient has a maximum, reaching the experimental and numerical records the highest shape similarity. It can also be seen that there is another parameter value that yields the highest amplitude similarity, in which the numerical record has the same RMS acceleration value as the experimental record. These two values are not coincident, adopting for the numerical model the strain hardening modulus value that produces the maximum cross-correlation coefficient since the difference between the RMS of the accelerations are less than 10%.

It can also be seen in the figure that the value of the hardening modulus that gives the highest similarity with the experimental results in numerical models with kinematic hardening ($\alpha = 3\%$) is significantly lower than the value that maximizes the correlation in models with isotropic hardening ($\alpha = 5\%$).

7. Experimental–numerical comparison

The structural accelerations of the numerical and experimental model in the time domain are compared in Fig. 11, while the comparison in the frequency domain can be seen in Fig. 12. The

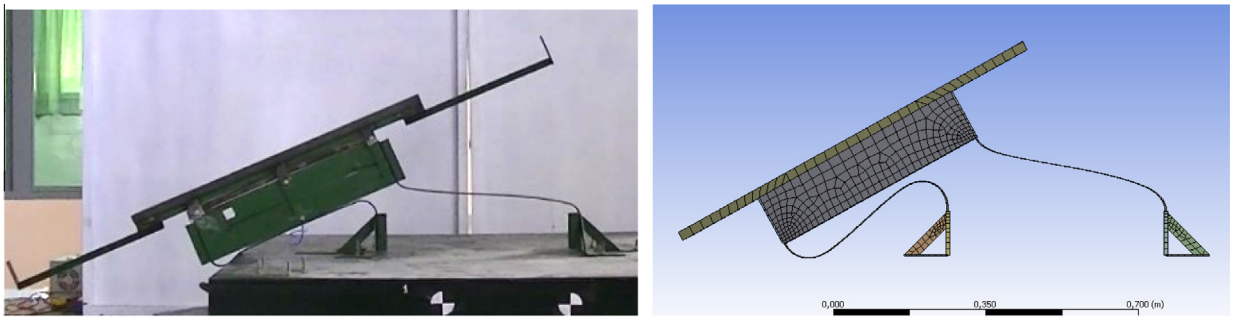

Fig. 9. Deformed shape after collapse of: (a) experimental model and (b) numerical model.

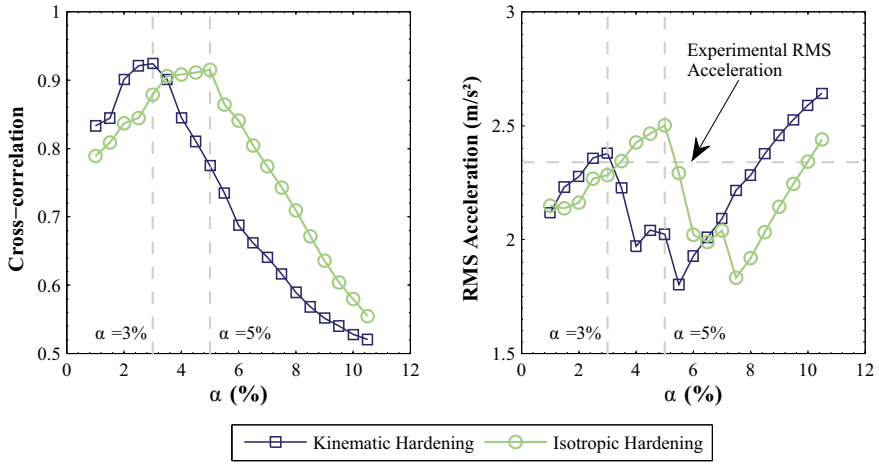

Fig. 10. Normalized cross correlation and RMS values of numerical and experimental acceleration records.

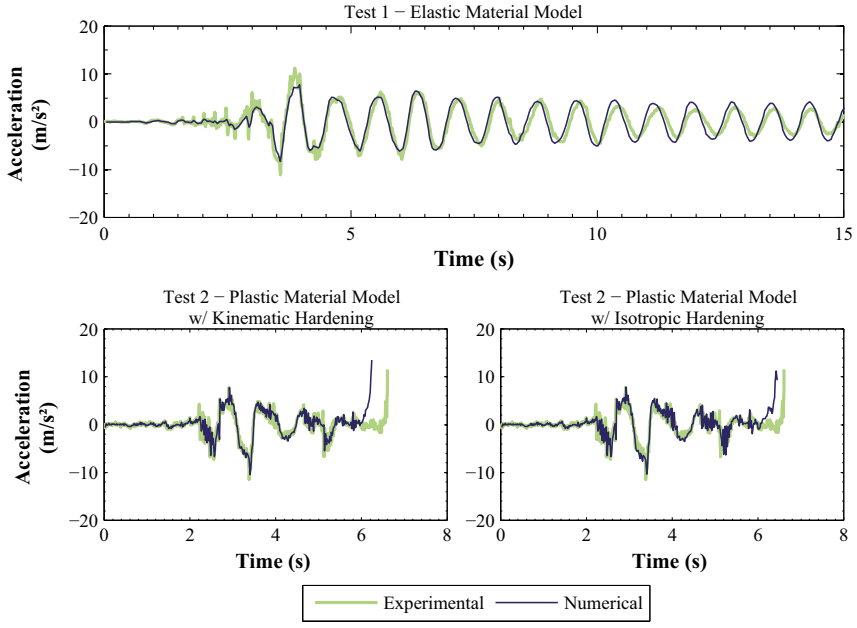

Fig. 11. Experimental–numerical comparison in the time domain.

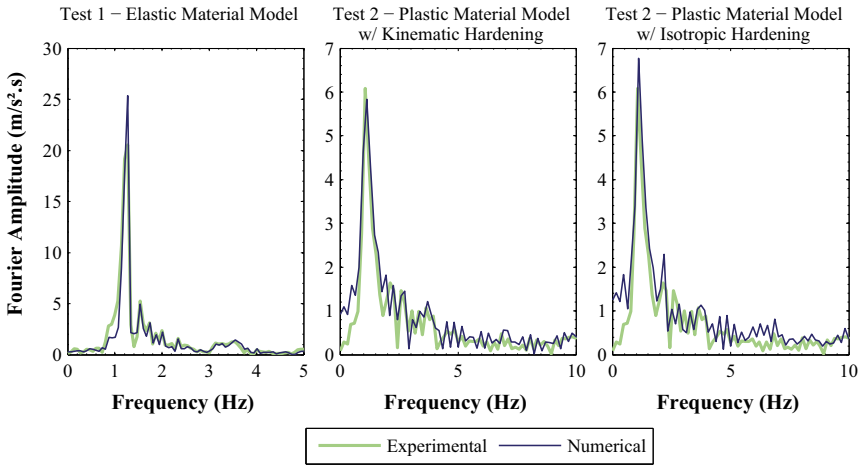

Fig. 12. Experimental–numerical comparison in the frequency domain.

summary of the results in terms of RMS and cross-correlation values are summarized in Table 6.

In general, a good correlation was noticed between numerical and experimental responses. In the case of the test 1, there are some amplitude differences and small offsets in time between responses once the strongest part of the seismic record takes place. In the case of test 2, differences can be observed mainly in the moment in which the structure collapses, observing the collapse of the numerical model in a shorter time than that observed experimentally. It can also be seen that the numerical model with kinematic hardening model reached a higher similarity in both shape and amplitude.

8. Influence of P-Delta effect on the structural collapse

In order to analyze the influence of P-Delta effect on the structural collapse a series of nonlinear dynamic analyzes were performed. The numerical models employed in this study are similar to those analyzed in the previous sections, with features listed in Table 7. In the models, different heights and thickness of the

Table 6
Results of the experimental–numerical comparison.

Test	Material model	RMS acceleration			Normalized cross correlation
		Experimental (m/s^2)	Numerical (m/s^2)	Relative difference (%)	
1	Elastic	3.11	3.22	3.39	0.927
2	Plastic with kinematic hardening	2.34	2.38	1.67	0.924
2	Plastic with isotropic hardening	2.34	2.50	6.92	0.915

Table 7
Properties of the structures analyzed.

Number of model	Column height (m)	Cross-section dimensions		Mass (kg)	Lateral stiffness		Fundamental frequency (Hz)	Stability factor
		Width (m)	Thickness (m)		w/P-Delta effect (N/m)	w/o P-Delta effect (N/m)		
1	0.49	2.54E−02	3.20E−03	33.85	2.17E+03	2.98E+03	1.28	0.23
2	0.55	2.54E−02	4.10E−03	50.00	3.21E+03	4.26E+03	1.28	0.21
3	0.69	2.54E−02	6.32E−03	100.00	6.40E+03	8.09E+03	1.28	0.18
4	0.86	2.54E−02	9.81E−03	200.00	1.28E+04	1.55E+04	1.28	0.15
5	1.04	2.54E−02	1.50E−02	400.00	2.56E+04	2.98E+04	1.28	0.13
6	1.21	2.54E−02	2.27E−02	800.00	5.16E+04	5.87E+04	1.28	0.11
7	1.29	2.54E−02	3.30E−02	1600.00	1.03E+05	1.16E+05	1.28	0.10

columns, as well as different values of concentrated mass in the beam were defined. This was done in order to obtain the same frequency in the fundamental mode of vibration and the same relationship between the seismic demand and the strength of the structure, while having different values in the stability factor. These stability factor values are greater than 0.1, the value at which, according to ASCE 7-10 [32], the P-Delta effect should be considered when member forces and story drifts are evaluated. At the same time, the stability factor values are below 0.25, the maximum value allowed by the ASCE 7-10. The properties of the material model employed are those obtained from the calibration described in the previous section.

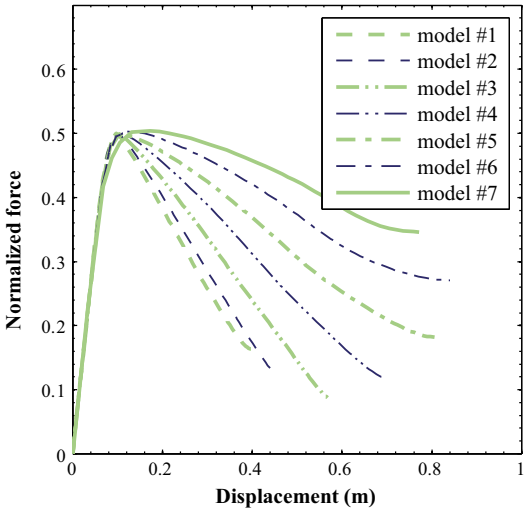

Fig. 13. Normalized force–displacement relationship for the analyzed structures.

The results of a pushover analysis of the different numerical models are shown in Fig. 13. The values of the horizontal forces applied on the analyzed structure are divided by the mass of the model in order to obtain the normalized force. Since the seismic demand can be characterized as the product of the spectral acceleration (same for all models) by the mass of each one of the analyzed structures, from Fig. 13 it can be inferred that all models employed in this study have the same relationship between strength and demand caused by the seismic action. It can also be seen in the figure as a higher factor of stability leads to a further decrease in the stiffness of the structure after reaching the maximum strength.

In order to compare the dynamic behavior of the different models, the minimum spectral acceleration that produces the structural collapse was sought for each seismic record. This characteristic value is found iteratively, modifying the amplitude of each record using the bisection method as detailed by Domizio [33].

With this value the collapse capacity (CC), defined according to Eq. (5), was calculated.

$$CC = \frac{S_a \cdot m}{f_y} \tag{5}$$

where S_a is the minimum spectral acceleration that produces the structural collapse, m is the mass of the structure and f_y is its yield strength. Fig. 14 shows the collapse capacity and the maximum ductility demand prior to collapse (μ_{max}) as a function of stability factor.

From the results of this analysis, the reverse relationship between the collapse capacity and the stability factor is observed. With both seismic records the collapse capacity was increased by approximately 60% when the stability factor decreased from 0.23 to 0.1. It was also observed that the collapse capacity is lower for

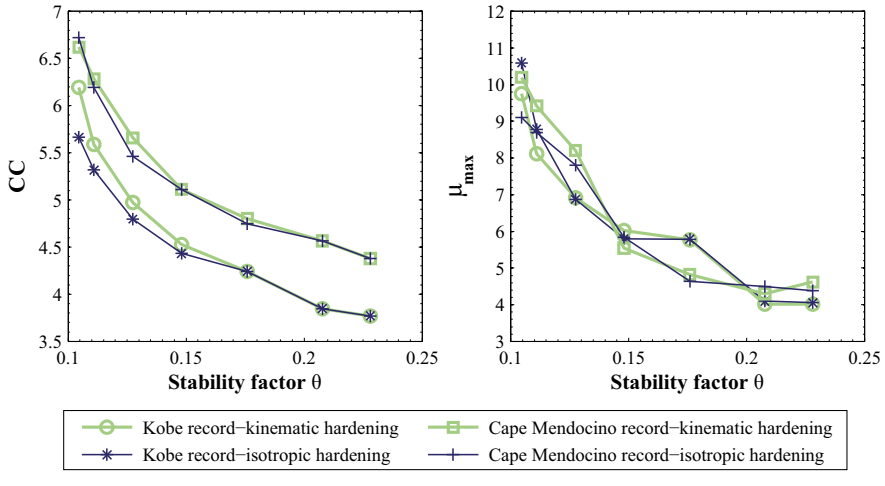

Fig. 14. Collapse capacity and maximum ductility demand related to stability factor.

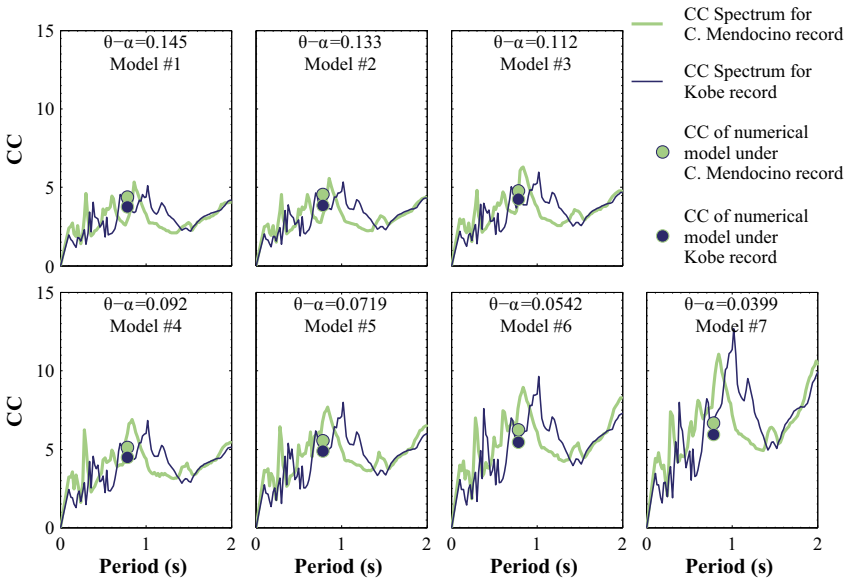

Fig. 15. Collapse capacity spectrums.

the Kobe earthquake, due to the higher frequency content near to the fundamental frequency of the structures analyzed.

In terms of the maximum demand of ductility, it can be seen in figure that, when the stability factor decreases from 0.23 to 0.1, the plastic deformation required to reach the structural collapse increase up to 160%. Compared to the analysis of the collapse capacity, smaller differences can be observed between the maximum ductility demands obtained with the two studied seismic records.

Again, no significant differences were observed between the results obtained using kinematic and isotropic hardening plasticity in the material model. This behavior is possibly due to the fact that the most of the plastic deformations occur in a few cycles, which is characteristic of near-fault earthquakes.

In order to compare the collapse capacity obtained in this study with that resultant of the methodology proposed by Adam and Jäger [17], a series of incremental dynamic analysis were performed. The structure was modeled as a SDOF spring-mass system where a bilinear force–displacement relationship with parameters defined from the pushover analysis presented in Fig. 13. From these results, the collapse capacity for a set of structures with different periods was established, forming the collapse capacity spectrums shown in Fig. 15. In this figure these results are compared with those obtained from the modeling described in the previous sections, and a considerable similarity between the results obtained with both methods can be observed. The collapse capacity proved to be somewhat higher in the structures modeled with the finite element method for larger values of stability factor and higher influence of P-Delta effect, noting the opposite in the case of structures with lower influence of P-Delta effect. The method by which the collapse capacity spectrum was performed is significantly less computationally expensive, and showed similar results to the method proposed in this paper, which was initially calibrated and compared with experimental results. This shows that it is a useful tool when assessing the collapse of structures of a degree of freedom that do not suffer cyclic degradation.

9. Conclusions

Throughout the present work the response of steel frame structures against near-fault seismic records was analyzed numerically and experimentally. These structures behave as dynamic systems of one degree of freedom and showed no stiffness degradation.

In the numerical simulations, the material model was defined by mean of a bilinear stress–strain relationship. Kinematic and isotropic hardening were defined and the results obtained with both type of hardening models were compared. The parameters were estimated from additional testing and calibration of the numerical model. In the calibration process it was observed that the response in the proximity of collapse is highly influenced by the strain hardening modulus defined in the material model.

In order to establish the degree of similarity between the experimental and numerical responses, the normalized cross-correlation and RMS values of the structural acceleration were employed as indicators. The first indicator measures the shape similarity of the records, while the second is a measure of the similarity in amplitude. The comparison in terms of RMS values showed a maximum relative difference less than 7%, while the minimum cross-correlation was greater than 0.91. Then it can be concluded that, with the exposed modeling methodology, it is possible to get responses from the numerical model that approximate acceptably the response measured in experimental tests, even when structures experience large plastic deformations and reach the collapse. This allows validating numerical models, making possible to accurately assess the seismic collapse capacity of the structure, requiring a realistic characterization of the component materials. On the other hand, it is remarkable that with the two criteria of strain hardening a good numerical/experimental correlation can be obtained, but different values of strain hardening modulus should be used. A percentage of the elasticity modulus of 3% should be used for kinematic hardening and a 5% should be used for isotropic hardening.

Finally, the influence of the P-Delta effect in the structural collapse was studied by a series of nonlinear dynamic analyzes, in which modeling methodology detailed in the previous section was followed. In these analyzes the amplitude of the seismic records was modified to find the lowest spectral acceleration that causes the collapse of the numerical model. In this study a series of structures similar to that analyzed in the numerical–experimental study were employed. These structures had equal fundamental frequency and strength-seismic demand ratio, but different stability factors, within the range in which the P-Delta effect should be

taken into account according to the ASCE-7. From the results of this study an inverse relationship between the stability factor and the collapse capacity, as well as between the stability factor and the maximum ductility demand prior to the collapse, were observed. For both analyzed seismic records, a decrease in stability factor from 0.23 to 0.10 was reflected in an increase of the collapse capacity about 60% and an increase about 160% of the ductility demand was also observed. Finally the results of this study were compared with the collapse spectrum built according to the methodology proposed by Adam and Jäger. A considerable similarity between the results obtained by both methods was observed, emphasizing the lower computational cost of the latter methodology.

Acknowledgements

The financial support of CONICET and the National University of Cuyo is gratefully acknowledged. Special acknowledgements are extended to the reviewers of the first version of the paper because their useful suggestions led to improvements of the work.

References

[1] Starossek U. Typology of progressive collapse. Eng Struct 2007;29:2302–7.
[2] Gupta A, Krawinkler H. Dynamic P-delta effects for flexible inelastic steel structures. J Struct Eng 2000;126:145–54.
[3] Villaverde R. Methods to assess the seismic collapse capacity of building structures: state of the art. J Struct Eng ASCE 2007;133:57.
[4] Haselton CB, Liel AB, Deierlein GG. Simulating structural collapse due to earthquakes: model idealization model calibration and numerical solution algorithms. In: Papadrakakis M, Lagaros ND, Fragiadakis M, editors. ECCOMAS thematic conference on computational methods in structural dynamics and earthquake engineering, Rhodes, Greece, 22–24 June 2009, COMPDYN 2009. p. 1–22.
[5] Liel AB, Haselton CB, Deierlein GG, Baker JW. Incorporating modeling uncertainties in the assessment of seismic collapse risk of buildings. Struct Saf 2009;31:197–211.
[6] Zareian F, Krawinkler H, Ibarra L, Lignos D. Basic concepts and performance measures in prediction of collapse of buildings under earthquake ground motions. Struct Des Tall Spec Build 2010;19:167–81.
[7] Eads L, Miranda E, Krawinkler H, Lignos DG. An efficient method for estimating the collapse risk of structures in seismic regions. Earthq Eng Struct Dyn 2013;42:25–41.
[8] Ibarra L, Krawinkler H. Global collapse of frame structures under seismic excitations; 2005.
[9] Haselton CB. Assessing seismic collapse safety of modern reinforced concrete moment frame buildings. Stanford University; 2006.
[10] Lignos DG, Chung Y, Nagae T, Nakashima M. Numerical and experimental evaluation of seismic capacity of high-rise steel buildings subjected to long duration earthquakes. Comput Struct 2011;89:959–67.
[11] Lignos D, Krawinkler H. Sidesway collapse of deteriorating structural systems under seismic excitations. John A. Blume Earthq. Eng. Center, Rep. No. 172, Stanford University, Stanford, USA; 2009.
[12] Bernal D. Instability of buildings during seismic response. Eng Struct 1998;20:496–502.
[13] Hjelmstad K, Williamson EB. Dynamic stability of structural systems subjected to base excitation. Eng Struct 1998;20:425–32.
[14] Grigorian M, Grigorian CE. Lateral displacements of moment frames at incipient collapse. Eng Struct 2012;44:174–85.
[15] Miranda E, Akkar S. Dynamic instability of simple structural systems. J Struct Eng ASCE 2003;129:1722–7.
[16] Shafei B, Zareian F, Lignos DG. A simplified method for collapse capacity assessment of moment-resisting frame and shear wall structural systems. Eng Struct 2011;33:1107–16.
[17] Adam C, Jäger C. Simplified collapse capacity assessment of earthquake excited regular frame structures vulnerable to P-delta. Eng Struct 2012;44:159–73.
[18] Kanvinde A. Methods to evaluate the dynamic stability of structures-shake table tests and nonlinear dynamic analyses. EERI Pap Compet 2003:1–12.
[19] Wu C, Loh C. Shake table tests on gravity load collapse of low-ductility RC frames under near-fault earthquake excitation. Adv Exp Struct 2006:725–32.
[20] Xuewei C, Xiaolei H, Cheang J, Shengyi L, Guiniu M. Dynamic inelastic numerical simulation for a shaking table test of a full scale steel moment frame structure based on OpenSEES. In: 14th World conf earthq eng, vol. 1, Bejing, China, October 2008.
[21] Yamada S, Suita K, Tada M, Kasai K. Collapse experiment on 4-story steel moment frame: Part 1. Outline of test results. In: 14th World conf earthq eng, Beijing, China, October 2008.
[22] Elwood K, Moehle J. Shake table tests and analytical studies on the gravity load collapse of reinforced concrete frames. Rep. 2003/01, Pacific Earthquake Engineering Research Center, Univ. of California, Berkeley, Calif.; 2003.
[23] Vian D, Bruneau M. Tests to structural collapse of single degree of freedom frames subjected to earthquake excitations. J Struct Eng ASCE 2003;129:1676–86.
[24] Lignos D, Krawinkler H. Prediction and validation of sidesway collapse of two scale models of a 4-story steel moment frame. Earthq Eng Struct Dyn 2011:807–25.
[25] Lignos DG, Hikino T, Matsuoka Y, Nakashima M. Collapse assessment of steel moment frames based on E-Defense full-scale shake table collapse tests. J Struct Eng ASCE 2012:461.
[26] Suita K, Yamada S, Tada M, Kasai K, Matsuoka Y, Shimada Y. Collapse experiment on 4-story steel moment frame: Part 2 detail of collapse behavior. In: Proc 14th world conf earthq eng, Beijing, China; 2008. p. 11.
[27] Ibarra L, Krawinkler H. Global collapse of frame structures under seismic excitations. Blume TR 152, Blume Earthq Eng Center, Stanford Univ; 2005.
[28] ANSYS 13. Theory reference. Canonsburg: ANSYS, Inc; 2010.
[29] Cao J, Lee W, Cheng HS, Seniw M, Wang H-P, Chung K. Experimental and numerical investigation of combined isotropic–kinematic hardening behavior of sheet metals. Int J Plast 2009;25:942–72.
[30] Yoshida F, Uemori T. A model of large-strain cyclic plasticity describing the Bauschinger effect and workhardening stagnation. Int J Plast 2002;18:661–86.
[31] Clough RW, Penzien J. Dynamics of structures. 3rd ed. Berkeley (USA): Computers & Structures, Inc.; 2003.
[32] ASCE 7-10. Minimum design loads for building and other structures; 2010.
[33] Domizio MN. Análisis numérico y experimental del desempeño de amortiguadores de masa sintonizada frente a sismos de falla cercana, M. Eng. dissertation. National University of Cuyo, Mendoza, Argentina; 2013.